



**ARTICLE**

## Study on Air-Purifying Performance of Semi-Flexible Asphalt Samples Coated with Titanium Dioxide Using Different Methods

Shoujing Yan<sup>1</sup>, Yangyang Wang<sup>2,\*</sup>, Fengxia Chi<sup>1</sup>, Xue Luo<sup>2</sup>, Tianjie Zhang<sup>3</sup> and Chenchen Xi<sup>1</sup>

<sup>1</sup>Institute of Road Engineering, Zhejiang Scientific Research Institute of Transport, Hangzhou, 310023, China

<sup>2</sup>Department of Architecture and Civil Engineering, Zhejiang University, Hangzhou, 310027, China

<sup>3</sup>Department of Computer Science, Boise State University, Boise, 83725-1145, USA

\*Corresponding Author: Yangyang Wang. Email: profxnzhang@126.com

Received: 19 May 2021 Accepted: 12 July 2021

### ABSTRACT

Titanium dioxide (TiO<sub>2</sub>) was recently employed to apply onto road surfaces to degrade the harmful compounds from vehicle emissions. However, it remains a challenging task to find a highly compatible pavement type for TiO<sub>2</sub> application to achieve durable and efficient air-purifying performance. This study proposed to coat TiO<sub>2</sub> particles onto semi-flexible pavement surface and tried to investigate an optimum coating method. Three coating methods, including direct mixing TiO<sub>2</sub> (MT) with asphalt mixture, spraying dry TiO<sub>2</sub> (ST) coating and water-solution-based TiO<sub>2</sub> (WT) coating on semi-flexible pavement surface. To achieve this objective, semi-flexible samples were prepared to evaluate and compare the performances of three coating methods by employing resistance to wearing, NO removal efficiency tests and residual texture depth tests. It was found that the ST method not only provided better NO degrading efficiency but also improved the resistance to wearing than the other two methods.

### KEYWORDS

Titanium dioxide; air-purifying performance; semi-flexible pavement; coating methods

## 1 Introduction

The quantity of vehicle keeps increasing rapidly in large cities, which emitted hundreds of millions of tons of vehicle emissions each year. Automobile exhaust contains a large number of harmful substances, including CO, NO<sub>x</sub>, SO<sub>2</sub> and other harmful gas components, which is one of the culprits of air pollution [1,2]. The high concentration of vehicle emissions is particularly terrible when vehicles start or change speed, which brings serious harm to the surrounding environment and the health of residents [3,4]. Thus, effective and efficient approaches to degrade the NO<sub>x</sub> as soon as they are emitted from vehicles are keenly desired.

Titanium dioxide (TiO<sub>2</sub>) has many advantages such as highly stable chemically, super-hydrophilicity and relatively low price. It makes TiO<sub>2</sub> an ideal photocatalytic material in construction engineering [5–7]. Many reports have demonstrated the feasibility of this material to decrease NO<sub>x</sub> concentration since its photocatalytic oxidation property was first discovered by Fujishima and Honda in 1972 [8]. In the 1980s, organic pollution in wastewater was degraded by adding TiO<sub>2</sub> and under high-intensity UV light [9,10].



The application of TiO<sub>2</sub>, especially the anatase phase titanium dioxide with high activity, as air-purifying materials originated in Japan [11,12]. Since then, a wide variety of products emerged on the market for indoor formaldehyde cleaning as well as for building facade applications. However, the dramatic increase in vehicle emissions in cities is seriously polluting air quality and is gradually attracting the attention of road engineering researchers [13–15].

In recent years, to improve the application scope of TiO<sub>2</sub>, attempts have been made to add it to pavement surfaces. It has been well demonstrated that coating TiO<sub>2</sub> particles onto road surface is an effective and efficient approach to purify the atmosphere [16,17]. There are two common approaches to add it onto road surfaces. One method is to replace equal quality of mineral powder with TiO<sub>2</sub> particles, which is considered as MT coating method [18]. The other common method is called WT coating method, which takes the TiO<sub>2</sub> particles dissolving into water and spraying it onto road surface [19]. But some previous studies have pointed out that MT has lower degrading performance than WT since the photocatalytic process will be active when TiO<sub>2</sub> direct contact with ultraviolet (UV) radiation and pollutants [20–22]. In contrast, TiO<sub>2</sub> particles in the WT coating method are easy to take away due to lack of sufficient adhesion, when a vehicle is driving at high speed. Hence, the anti-wearing ability and sustainable degradation of WT are extremely poor compared with MT. In order to enhance the adhesion between TiO<sub>2</sub> particles and road surface, the researchers in Hong Kong applied chemical means to fabricate numerous microspores on the surface of asphalt film, and TiO<sub>2</sub> particles self-assemble into the micropores driven by the surface convection and capillary force [23,24]. The porous TiO<sub>2</sub> coating is donated as porous TiO<sub>2</sub> (PT) method, which is fabricated through Breath Figure (BF) process [25]. The reports have shown that PT method has higher purification efficiency and stronger anti-wearing ability on asphalt pavements [26–28]. But its preparation process is very complex causing difficulty to promote on a large scale in engineering. Thus, it has great significance to develop an innovative method, which not only has durable and efficient air-purifying performance, but also has excellent anti-wearing ability.

The main objective of this study is to develop an approach should be provided with high sustainable degrading ability and anti-wearing performance. To achieve this objective, rutting plate specimens were first prepared and coated using MT, WT and ST methods. Then, NO degradation efficiency, anti-wearing ability and residual texture depth of specimens were measured by vehicle emission test equipment, kneading machine and, laser scanner, respectively.

## 2 Experimental Preparations

### 2.1 Materials

Rutting plate specimens (length = 300 mm, width = 300 mm and height = 50 mm) were prepared. A porous asphalt mixture (void ratio is 24%) was designed. The SBS modified asphalt was used and the asphalt content was 4.3%. All rutting plates were compacted by asphalt mixture electro-hydraulic wheel crushed machines according to T 0703, JTG E20-2011. Table 1 shows the detailed information of custom-designed cement grouting material.

**Table 1:** Components of cement grouting material

Materials	Hydrae cement	Mineral powder	Expansion agent	Water reducer	Accelerator	Water-binder ratio
Rate/%	0.9	0.1	0.08	0.01	0.005	0.5

## 2.2 TiO<sub>2</sub> Coating Process

Table 2 describes the process for preparing the TiO<sub>2</sub> coating materials using MT, WT and ST methods. All coating materials were prepared at room temperature ( $25 \pm 1^\circ\text{C}$ ) and humidity ( $50\% \pm 3\%$ ). As for MT, the mineral powder in asphalt mixture was replaced by TiO<sub>2</sub> particles with equal quality. For WT, the equal quality TiO<sub>2</sub> (mass ratio of TiO<sub>2</sub> and water = 0.5:100) was dissolved into water directly and sprayed it on surface of specimens. Specially, ST compared with WT for different spraying occasions since ST sprayed dry TiO<sub>2</sub> particles before cement grouting material was initially setting, while WT sprayed TiO<sub>2</sub> coating solution after that was finally setting. Each group has three samples and equal quality of TiO<sub>2</sub>. Blank group (BG) has no TiO<sub>2</sub> prepared to control experimental reliability. As a result, expect for BG, each specimen has approximately 40.015 g of TiO<sub>2</sub> particles.

**Table 2:** Rutting plates with different coating methods

Group ID	Sample amount	TiO <sub>2</sub> mass/g	Coating process
BG	3	0	–
MT	3	40.015	Mixing TiO <sub>2</sub> into asphalt mixture
WT	3	40.015	Spraying TiO <sub>2</sub> coating solution onto samples surface
ST	3	40.015	Embedding TiO <sub>2</sub> particles onto samples surface

It is worth to note that an innovative method ST is inspired by PT method. TiO<sub>2</sub> particles through chemical adhesive which is generated during cement grouting material solidification. The procedure of ST method can be described as follows:

- (A) Preparing rutting plates of porous asphalt mixture;
- (B) Compounding custom-designed cement grouting material into rutting plates;
- (C) Cleaning the cement grouting material on the surface of the asphalt mixture until the coarse aggregate exposed;
- (D) The TiO<sub>2</sub> particles are homogeneously spared onto rutting plate before cement grouting material initial setting by using electric duster;
- (E) Before cement grouting material finally setting, cleaning the free TiO<sub>2</sub> particles in the surface of the coarse aggregate. The TiO<sub>2</sub> particles are embedded onto the cement grouting material in road surface texture.

The specific preparation steps of ST method are shown in Fig. 1.

TiO<sub>2</sub> has a discontinuous band structure with a band gap between the valence band and the conduction band [29,30]. Once photon energy TiO<sub>2</sub> absorbed is larger than its band gap, the e<sup>-</sup> on the valence band reaches the excited state and migrates to the conduction band [31,32]. Then, the valence band produces strong reducibility, while the conduction band lacks electrons to generate h<sup>+</sup> with strong oxidizing property. Water and hydroxide ions (OH<sup>-</sup>) are adsorbed when they contact the surface of TiO<sub>2</sub> particles, which can react with h<sup>+</sup> to produce a more powerful oxidant [33,34]. In addition, oxygen (O<sub>2</sub>) in the air captures electrons to form O<sup>2-</sup>, which also is highly active oxidant. When vehicle passes the road coating TiO<sub>2</sub>, some harmful gases (NO, CO, etc.) in automobile exhaust combined with ·OH and O<sup>2-</sup>, which were oxidized to NO<sub>2</sub>, CO<sub>2</sub> and H<sub>2</sub>O. Both NO and NO<sub>2</sub> could be degraded to water and generated final product, nitric acid (HNO<sub>3</sub>), which could be easily flushed away by rainwater. The photocatalytic degradation process of titanium dioxide is shown in Fig. 2.

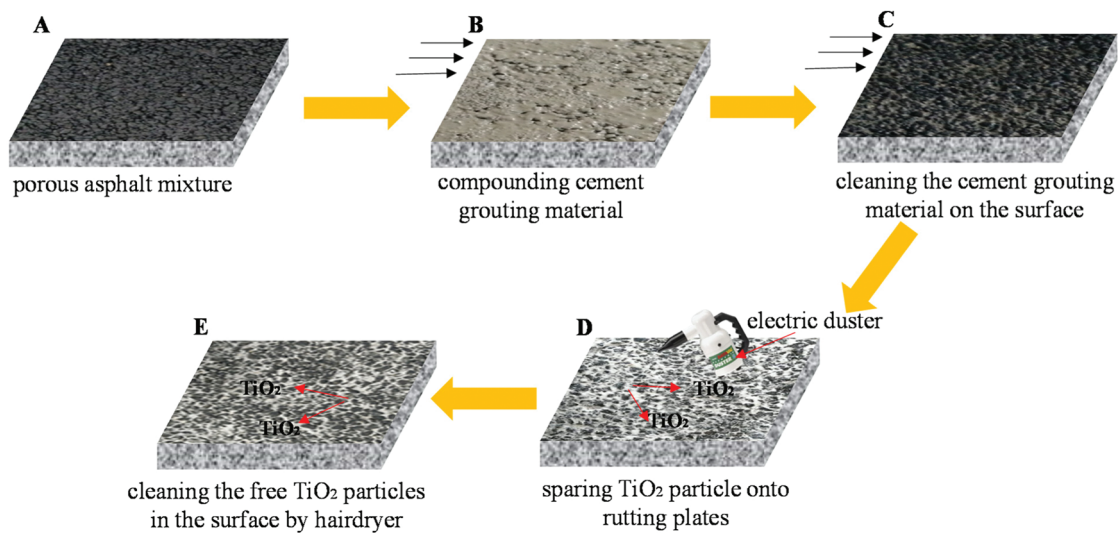


**Figure 1:** ST coating process: (A) preparing rutting plates of porous asphalt mixture; (B) filling cement grouting material; (C) cleaning the cement mortar on the surface of the asphalt mixture; (D) sparing  $\text{TiO}_2$  particles before cement grouting material initial setting; (E) when the cement grouting material is finally setting,  $\text{TiO}_2$  particles embed onto pavement surface

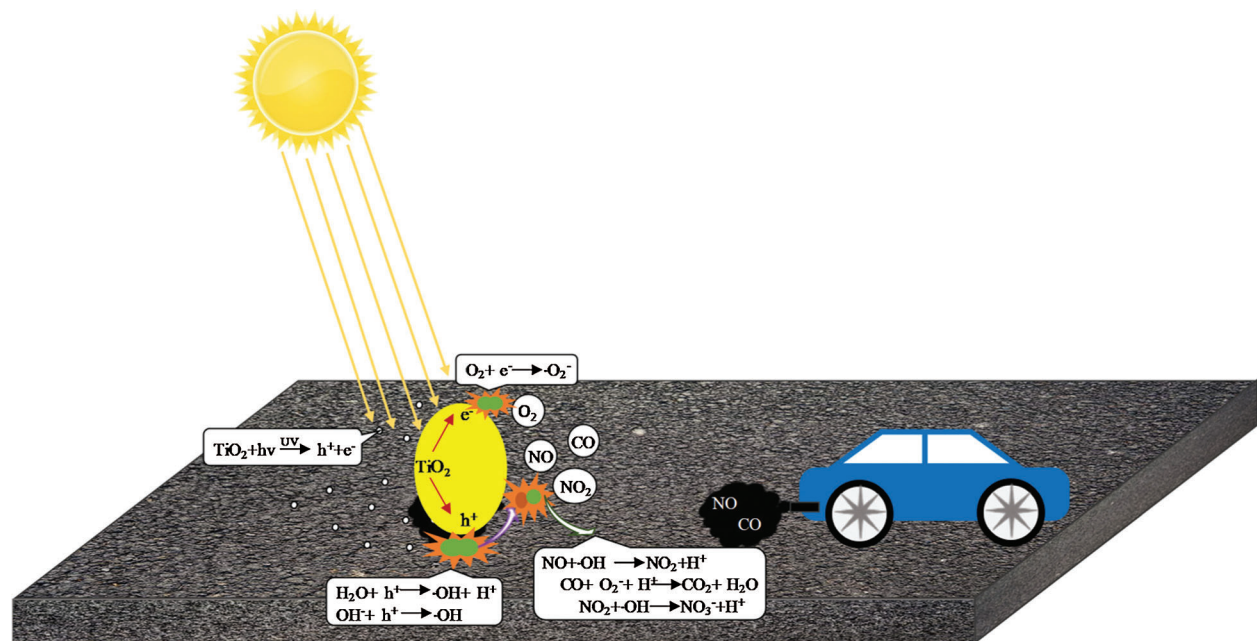


**Figure 2:** Photocatalytic process of  $\text{TiO}_2$  on road surface

### 3 Experiments and Methods

#### 3.1 No Degradation Efficiency Test

The  $\text{TiO}_2$  coating on pavement surface is easily carried off by vehicle [35]. Hence, it is important to measure its residual photocatalytic degradation performance according to GB18285-2018. In this paper, the custom-designed vehicle emission testing equipment was used to assess NO degradation ability of

different TiO<sub>2</sub> coating methods. Fig. 3 shows the vehicle emission testing system, which consists of vehicle emission collector, reacting chamber, UV lights and gas analyzer. The size of the reacting chamber is 500 mm × 500 mm × 400 mm, which was made of polymethyl methacrylate (PMMA) with excellent light transmission performance. Three ultraviolet lamps were parallel placed on the top of chamber and the distance of each lamp was adjusted until UV intensity achieved 30 W/m<sup>2</sup> when contacting sample's surface, which was very similar to that from sunlight in Zhejiang Province. The exhaust emission concentration was recorded by gas analyzer and the temperature and humidity inside reacting chamber were controlled at 25 ± 5°C. The residual degradation efficiency is calculated by Eq. (1)

$$RDE = \frac{C_{X,0} - C_{X,1}}{C_{X,0}} \times 100\% \quad (1)$$

where RDE is residual degradation efficiency; C<sub>x, 0</sub> and C<sub>x, 1</sub> are initial and stable concentration vehicle emission concentration after X hours of repeat abrasion, respectively.

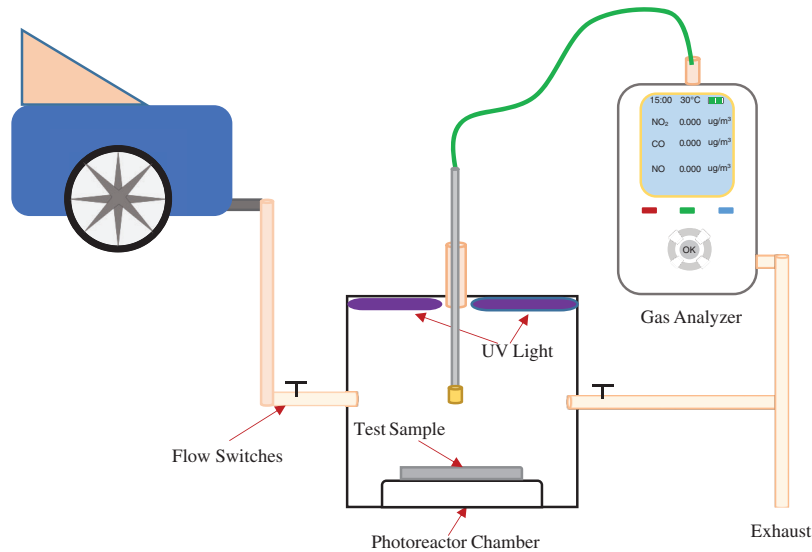


**Figure 3:** Composition of vehicle emission testing system

### 3.2 Anti-Wearing Ability Test

The sustainability photocatalytic degrading performance of TiO<sub>2</sub> coated on road surface mostly depends on tire abrasion [36,37]. Thus, it is necessary to evaluate the anti-wearing ability formed between TiO<sub>2</sub> particles and cement grouting materials. In this paper, the kneading machine was employed to simulate tire abrasion process, as shown in Fig. 4a. Fig. 4b presents the tire wearing routes on specimens. The most outstanding advantage of the kneading machine is that it can provide the friction in the forward direction and the lateral shear force, compared with traditional rutting test machine. Before applying abrasion, the air temperature in kneading machine was controlled at 60 ± 5°C. Then, the rutting plates coating TiO<sub>2</sub> were fixed on kneading machine, when its temperature stable at 60 ± 1°C. The tire was positioned in contact with the specimen surface and wore it back and forth at a frequency of 30 times per minute. The anti-wearing ability was calculated by Eq. (2).

$$AWA = \frac{M_X}{M_0} \times 100\% \quad (2)$$

where AWA is anti-wearing ability;  $M_x$  is the sample mass after  $x$  hours of abrasion;  $M_0$  is original sample mass. A higher of AWA present a better anti-wearing ability of  $TiO_2$  coating methods.

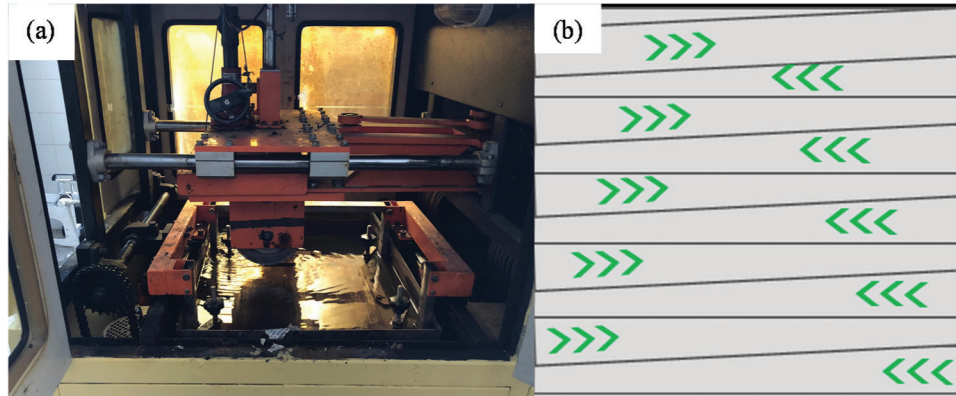


**Figure 4:** Wearing process: (a) kneading machine; (b) tire wearing routes

### 3.3 Residual Texture Depth Test

The texture depth of  $TiO_2$  coating samples decreased rapidly with increasing tire abrasion times. Thus, it is necessary to test the texture depth. The laser scanner can accurately measure the three-dimensional profile on the surface of the specimen [38]. In this study, high precision laser scanner, maximum scanning accuracy exceed 0.5 mm, was applied to evaluate the residual texture depth every 4 h, as shown in Fig. 5. The specimens were scanned by laser to obtain its texture depth from abrasion beginning to finish. Then the texture depth was calculated by Eq. (3)

$$RTD = \frac{T_X}{T_0} \times 100\% \quad (3)$$

where  $RTD$  is residual texture depth;  $T_X$  is the sample texture depth after  $x$  hours of abrasion;  $T_0$  is original texture depth of sample.

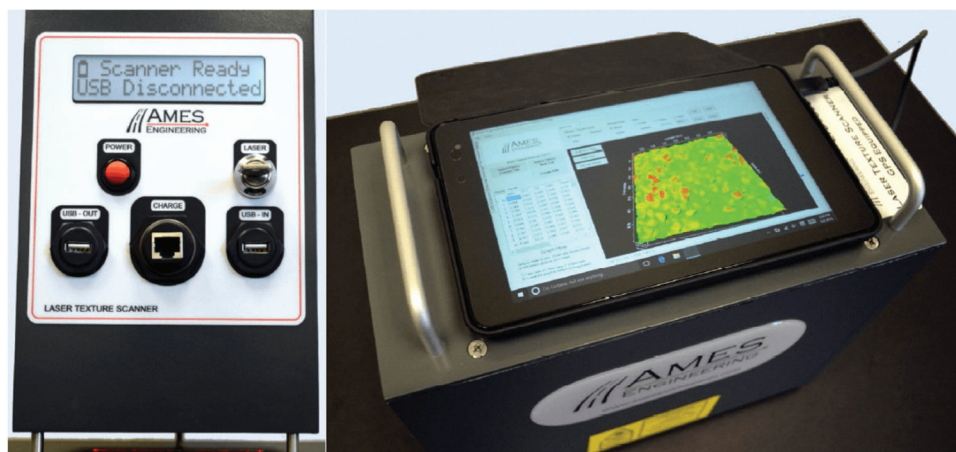


**Figure 5:** Laser scanner

## 4 Result and Discussion

### 4.1 No Degrading Efficiency Test Results

Fig. 6 shows the average NO degrading efficiency test results of all samples with various hours of tire abrasion. For BG specimens, the average NO depuration ability is almost zero, which illustrates that NO is not degraded without  $\text{TiO}_2$  particles. WT and ST samples had similar average RDE values (86.573% and 85.671%), which are much higher than that of MT specimens (1.941%). It is worth to notice that the degrading efficiency of WT is slightly higher than ST in the initial stage. However, the NO degrading efficiency of WT drops drastically since the average RDE value declines from 86.573% to 79.549%, which declines much faster than ST (85.671% to 85.403%) within 4 h. It can be clearly seen that there is an obvious decrease in RDE for WT and MT specimens, which are declined 22.223% and 10.46%, respectively, compared to its initial state. While, there are only 1.292% drops for ST specimens after 12 h of abrasion.

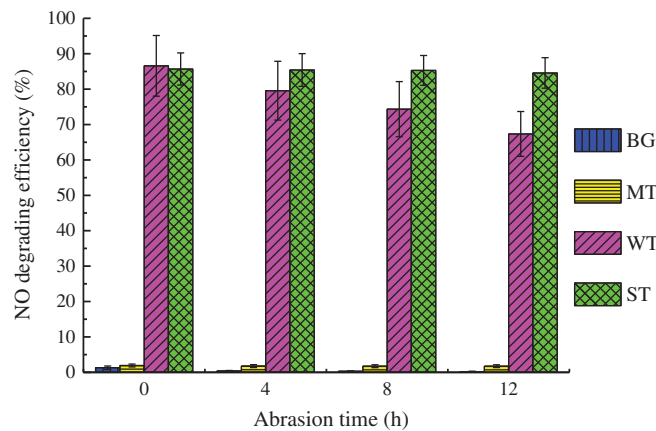
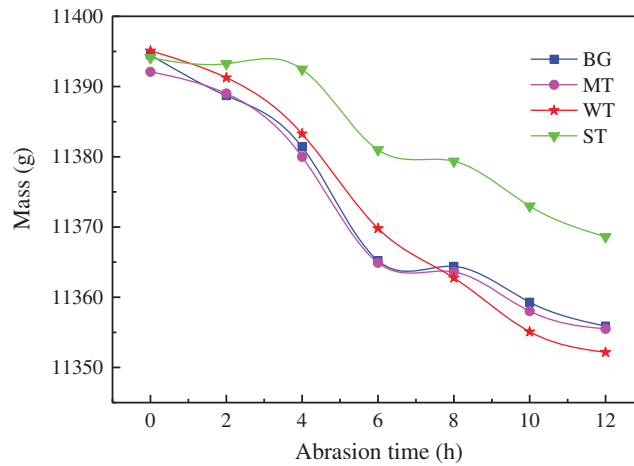


**Figure 6:** No degrading efficiency test results

The above test results indicated that WT has higher degrading efficiency in the initial stage, while ST had better sustainable degrading ability than other coating methods. The unsatisfactory residual degradation efficiency of WT mainly attributed to poor adhesion between  $\text{TiO}_2$  particles and cement grouting materials, because  $\text{TiO}_2$  particles are easily taken away by tire abrasion. Conversely, the excellent sustainable degrading performance of ST primary comes from cement grouting materials provided strong adhesion.

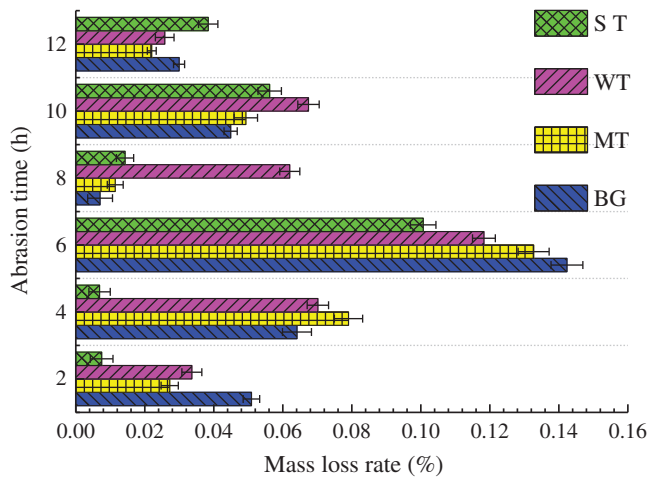
### 4.2 Anti-Wearing Ability Test Results

Fig. 7 represents the average anti-wearing ability results of specimens. It can be observed that the average mass of all samples decreased with varying abrasion time. The specimens in BG group and MT group have similar AWA values which are lower than that of WT specimens. The mass losing rate of ST group specimens decreased the slowest compared to other groups, indicating that ST coating method has the highest anti-wearing ability. However, samples in WT group have the same mass  $\text{TiO}_2$  particles compared to other coating methods, provided the biggest AWA values, suggesting the poorest anti-wearing ability.



**Figure 7:** Mass variation of specimens inside the kneading machine

The results in Fig. 8 also indicated that ST group specimens have better anti-wearing performance. The mass dropped rapidly and the mass losing rate, for all groups, reached its peak from 4 to 6 hours abrasion. In this stage, the mass losing rate of BG, MT, WT and ST are 0.142%, 0.133%, 0.118% and 0.101%, respectively. In addition, although WT performed better than BG and MT at the original stage, its performance deteriorates dramatically after 4 h abrasion. The anti-wearing ability of ST is 0.224% after 12 h abrasion, whereas that of BG, MT and WT are 0.339%, 0.321% and 0.376%, respectively. A phenomenon to be noted is that the ST group specimens have lower mass loss rate in the initial stage of abrasion test (2–4 h), but have the higher mass loss rate at the final stage (12 h). The reason for this phenomenon is that the cement grouting material firmly adheres to the TiO<sub>2</sub> particles by strong chemical coagulation force, in initial stage of abrasion. With increasing of wearing times, the increased loss rate of TiO<sub>2</sub> particles is due to the cement grouting material on the surface layer gradually worn out.



**Figure 8:** Mass losing rate of samples

The enhanced anti-wearing ability of ST coating method is primarily attributed to the adhesive from cement grouting materials initial setting. When grouting materials finally setting,  $\text{TiO}_2$  particles firmly embedded onto semi-flexible pavement surface results in  $\text{TiO}_2$  particles are not easily be taken away by the tire. The specimens in WT group have the poorest ability of abrasion due to its poor adhesion between  $\text{TiO}_2$  and road surface.

### 4.3 Residual Texture Depth Test Results

Figs. 9–12 describes the 3D point cloud images obtained the retention texture depth accurately of all specimens through laser scanner. The 3D point cloud is imaged by the relative height of object, the redder the image represents the higher the height, and the bluer the image represents the lower the height. It can be observed that the 3D point cloud images of all groups have similar profiles before tire abrasion, while show significant differences of each group after 12 h of abrasion.

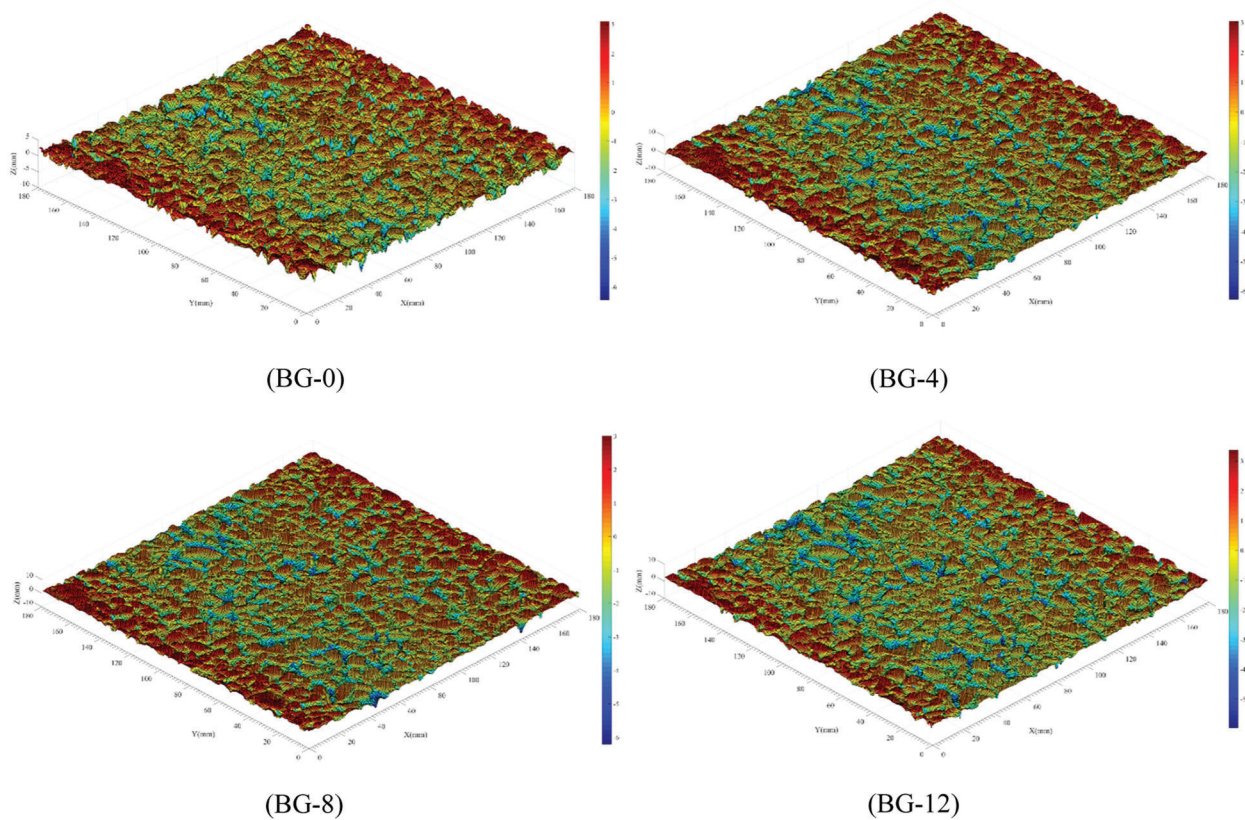


**Figure 9:** 3D point cloud images of BG group

For BG specimens, the red area of BG-0 image accounts for large area the whole image than blue area. After 4 h of abrasion, the blue area in the 3D point cloud image grew rapidly. The color of the blue area in the 3D point cloud image gradually changes from light blue to dark blue with 8 h of abrasion. BG-12 depicts the 3D point cloud image after 12 h of abrasion, and the blue area in this image is significantly larger than the red area. This phenomenon indicates that the texture depth will decline gradually with the increase of the abrasion time.

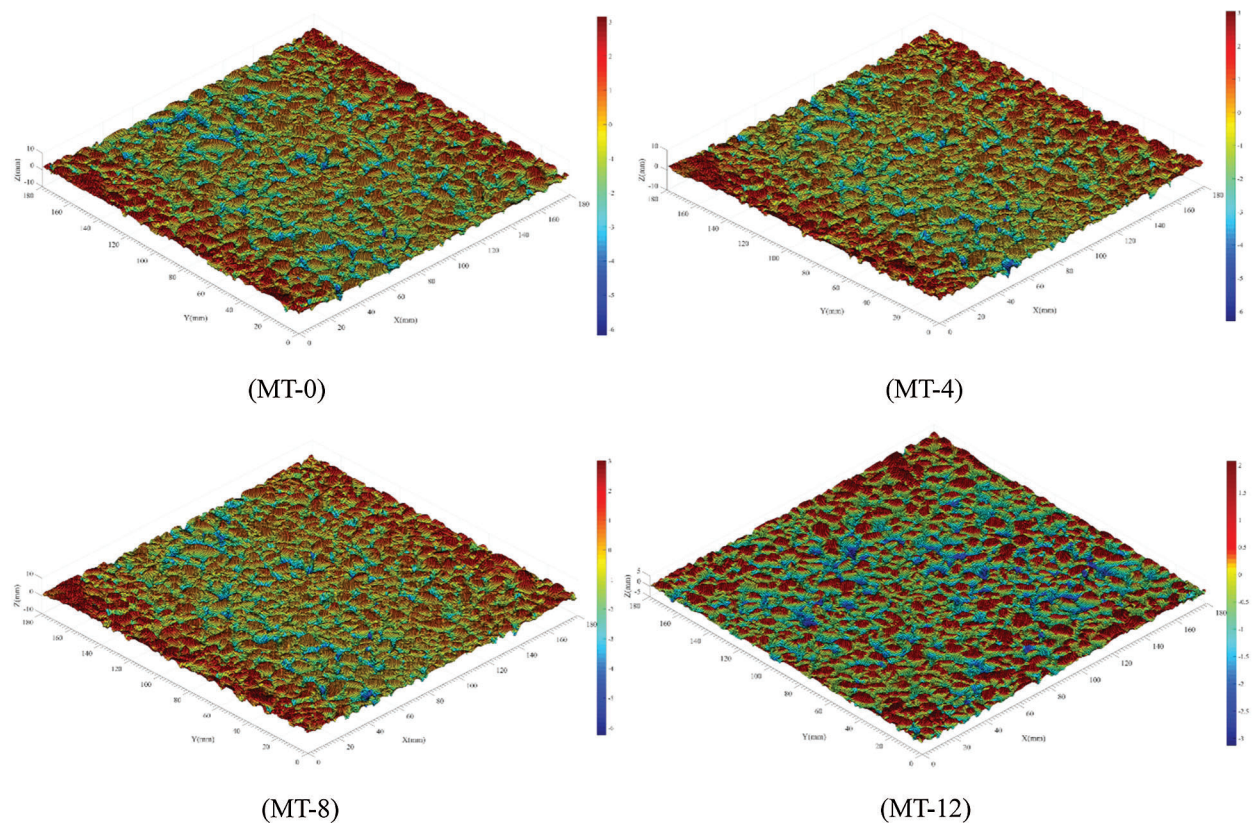
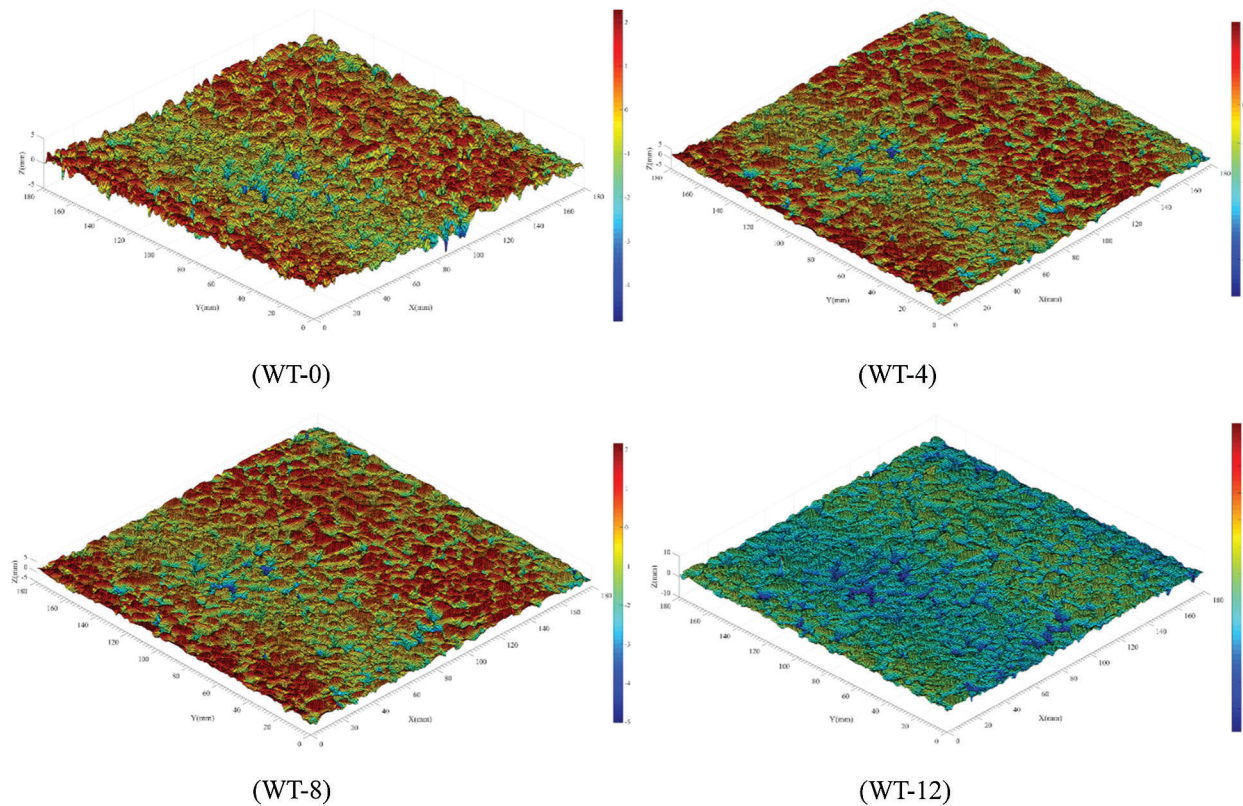


**Figure 10:** 3D point cloud images of MT group

Fig. 10 presents the changes of 3D point cloud images of MT group. It is obvious that the 3D profile and color trends of MT group is very similar to BG group. This is due to the fact that MT specimens replaced the mineral powder with titanium dioxide nanoparticles in equal volume during asphalt mixture forming process. Therefore, the changes in 3D profile of specimens are consistent between two groups during the abrasion process.

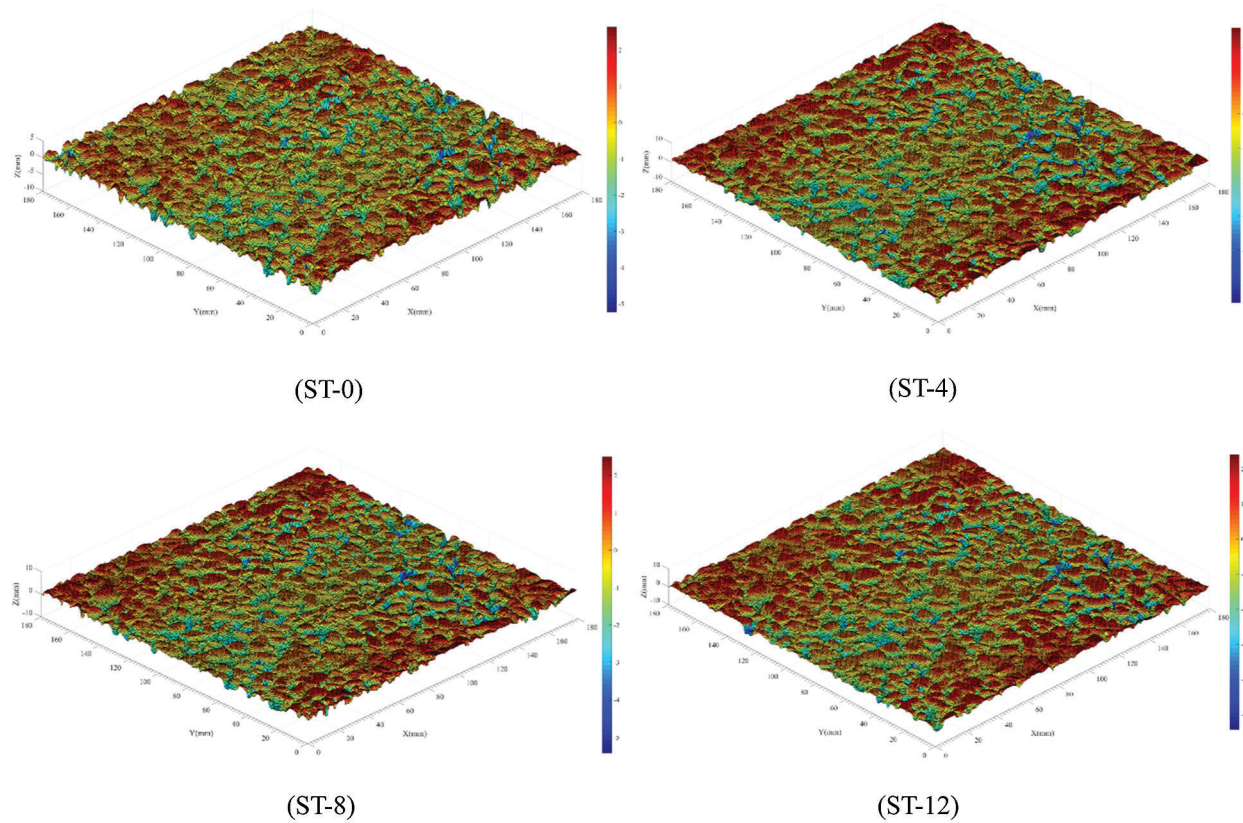
For WT specimens, the trends of 3D point cloud images are extremely different compared with BG and MT groups. The texture depth declined dramatically during the first 8 h wearing process. After 12 h abrasion, blue area takes up almost the entire picture, and there are some dark blue areas on the middle of MT-12 image. The above phenomenon shows that the material on surface layer of WT specimens is extremely shed during abrasion process.

Fig. 12 presents the trends of 3D point cloud image of the ST specimens. It can be clearly seen that the variations between every 3D point cloud image is minor. Comparing with ST-0, ST-4, ST-8 and ST-12, the images are basically red areas and not appear blue areas. It shows that the structure depth of the specimen hardly decreases during the wearing process.



**Figure 11:** 3D point cloud images of WT group

Fig. 13 summarizes the average retention texture depth of samples with various coating methods. Compared to the initial state, the RTD of WT group has the fastest decline and that of the ST group decreased the slowest. During the first 4 h of wearing, the RTD value of the specimens in the WT group decreased 0.045%, which was 0.023%, 0.019% and 0.037% higher than the BG, MT and ST groups during the same period, respectively. It is because is that after 4 h of abrasion, the amount and distribution of the  $\text{TiO}_2$  particles at MT and ST specimen surfaces became relatively stable. In addition, after 12 h abrasion, there were only minor drops in ST specimens, but significant drops in WT specimens. The average RTD values of BG, MT and ST were 0.961%, 0.962% and 0.979%, respectively, while only 0.941% for WT group. Future more, the rate of RTD decline was higher in BG and MT groups than ST group, and both showed a high similarity in decline trend. The reason for this phenomenon is that MT specimens replaced the mineral powder with titanium dioxide nanoparticles in equal quality during asphalt mixture forming process. Therefore, the trends of RTD curves and the corresponding 3D point cloud image changes of the specimens in BG and MT groups are consistent. It can also be noticed the ST specimens provided the highest RTD value at all stages. In other words, ST coating methods provided better abrasion resistance than MT and WT methods.



**Figure 12:** 3D point cloud images of ST group

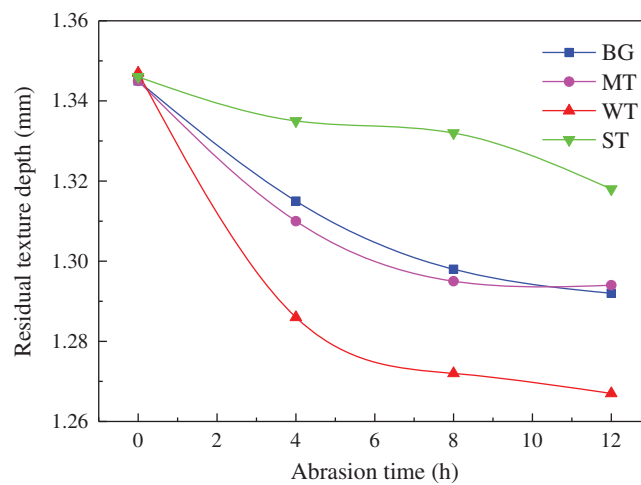


**Figure 13:** Average residual texture depth of specimens

## 5 Conclusions

In this paper, an innovative  $\text{TiO}_2$  coating method (ST) was proposed. The NO degradation efficiency, anti-wearing ability, and residual texture depth of three  $\text{TiO}_2$  coating methods (MT, WT and ST) were

analyzed to obtain sustainable air-purifying ability and anti-wearing performance on semi-flexible pavement. Based on the above experimental results, the main conclusions are shown as follows:

(1) In terms of NO degrading efficiency, WT has better purifying ability than MT and ST in the initial stage, while ST provides higher sustainable degrading ability than that of the other two methods.

(2) The ST method provide the best anti-wearing ability, followed by the MT method and WT method.

(3) Considering the NO removal efficiency and durability, the ST method has the best degrading efficiency, good anti-wearing property and better sustainable purification performance, which is the most promising coating method to semi-flexible pavement.

It should point out that this paper only considered the effect of wheel abrasion on sustainable air-purifying performance and residual structure depth. However, temperature and humidity are also very important factors. Hence, it is necessary to develop the coating erosion experiments with the coupled conditions of temperature, load and humidity in further research. More durable degrading performance, stronger anti-wearing materials and simpler coating methods should be developed to satisfy the urgent needs of degrading the vehicle emissions.

**Funding Statement:** The authors would like to acknowledge the Science Technology Department of Zhejiang Province (Grant Nos. 2018F10045 and 2021C01106) for the funding support and the technical guidance in 3D laser scanning by Dr. Fengxia Chi from the Institute of Road Engineering of Zhejiang Scientific Research Institute of Transport. The constant of this paper reflects the views of authors, who are responsible for the facts and the accuracy of the data shown herein. The authors gratefully acknowledge their financial and technical supporting.

**Conflicts of Interest:** The authors declare that they have no conflicts of interest to report regarding the present study.

## References

1. Tang, X., Wang, X., Yang, L., Zhang, Z. J., Wang, J. (2020). Multifunctional nickel nanofiber for effective air purification: PM removal and no reduction from automobile exhaust. *Journal of Materials Science*, 55(6), 6161–6171. DOI 10.1007/s10853-020-04383-2.
2. Kandimalla, P., Vatte, P., Bandaru, C. (2020). Phycoremediation of automobile exhaust gases using green microalgae. *Environment Development and Sustainability*, 23(3), 6301–6322. DOI 10.1007/s10668-020-00873-0.
3. Saran, S., Manjari, G., Devipriya, S. P. (2018). Synergistic eminently active catalytic and recyclable Ag, Cu and Ag–Cu alloy nanoparticles supported on TiO<sub>2</sub> for sustainable and cleaner environmental applications: A phytogenic mediated synthesis. *Journal of Cleaner Production*, 177, 134–143. DOI 10.1016/j.jclepro.2017.12.181.
4. Huang, Y., Wang, L., Zhang, S., Zhang, M., Ni, S. (2020). Source apportionment and health risk assessment of air pollution particles in eastern district of Chengdu. *Environmental Geochemistry and Health*, 42, 2251–2263. DOI 10.1007/s10653-019-00495-0.
5. Chavan, R. D., Yadav, P., Nimbalkar, A., Bhoite, S. P., Bhosale, P. N. et al. (2019). Ruthenium doped mesoporous titanium dioxide for highly efficient, hysteresis-free and stable perovskite solar cells. *Solar Energy*, 186, 156–165. DOI 10.1016/j.solener.2019.04.098.
6. Tan, W., Peralta-Videa, J. R., Gardea-Torresdey, J. (2018). Interaction of titanium dioxide nanoparticles with soil components and plants: Current knowledge and future research needs-a critical review. *Environmental Science: Nano*, 5(2), 257–278. DOI 10.1039/C7EN00985B.
7. Abdulhameed, A. S., Mohammad, A., Jawad, A. H. (2019). Application of response surface methodology for enhanced synthesis of chitosan triphosphosphate/TiO<sub>2</sub> nanocomposite and adsorption of reactive orange 16 dye. *Journal of Cleaner Production*, 232, 43–56. DOI 10.1016/j.jclepro.2019.05.291.

8. Skoutelis, C. G., Antonopoulou, M., Giannakas, A. E., Deligiannakis, Y., Konstantinou, I. K. (2016). Mechanism of synergistic photocatalytic Cr (VI)-reduction and benzoic acid oxidation by visible light active TiO<sub>2</sub> photocatalysts. *Journal of Advanced Oxidation Technologies*, 17(4), 202–211. DOI 10.1177/0022022180114007.
9. Tijani, J. O., Momoh, U. O., Salau, R. B., Bankole, M. T., Abdulkareem, A. S. et al. (2019). Synthesis and characterization of Ag<sub>2</sub>O/B<sub>2</sub>O<sub>3</sub>/TiO<sub>2</sub> ternary nanocomposites for photocatalytic mineralization of local dyeing wastewater under artificial and natural sunlight irradiation. *Environmental Science and Pollution Research*, 26, 19942–19967. DOI 10.1007/s11356-019-05124-y.
10. Wu, Y., Zhong, L., Yuan, J., Xiang, W., Chang, H. (2020). Photocatalytic optical fibers for degradation of organic pollutants in wastewater: A review. *Environmental Chemistry Letters*, 19(70), 1–12. DOI 10.1007/s10311-020-01141-3.
11. Tabatabaei, J., Gorji, L. (2019). The effect of TiO<sub>2</sub> nanoparticles in reduction of environmental pollution in concrete structures. *Advances in Concrete Construction*, 7(2), 127–129. DOI 10.12989/acc.2019.7.2.127.
12. Xu, M., Bao, Y., Wu, K., Xia, T., Li, V. C. (2019). Influence of TiO<sub>2</sub> incorporation methods on nox abatement in engineered cementitious composites. *Construction and Building Materials*, 221, 375–383. DOI 10.1016/j.conbuildmat.2019.06.053.
13. Jin, J., Xiao, T., Tan, Y., Zheng, J., Liu, R. et al. (2018). Effects of TiO<sub>2</sub> pillared montmorillonite nanocomposites on the properties of asphalt with exhaust catalytic capacity. *Journal of Cleaner Production*, 205, 339–349. DOI 10.1016/j.jclepro.2018.08.251.
14. Boyle, C., Skillen, N., Stella, L., Robertson, P. (2019). Development and optimization of an immobilized photocatalytic system within a stacked frame photoreactor (SFPR) using light distribution and fluid mixing simulation coupled with experimental validation. *Industrial And Engineering Chemistry Research*, 58(8), 2727–2740. DOI 10.1021/acs.iecr.8b05709.
15. Krylov, P. M., Volodin, O. N., Zaitsev, G. A., Nekrasova, L. P., Klyuchniko, V. et al. (2019). Estimating summer emissions from land transportation vehicles moving along the urban roads. *Asian Journal of Water, Environment and Pollution*, 16(4), 29–37. DOI 10.3233/AJW190046.
16. Kermani, M., Kakavandi, B., Farzadkia, M., Esrafil, A., Jokandan, S. F. et al. (2018). Catalytic ozonation of high concentrations of catechol over TiO<sub>2</sub>@Fe<sub>3</sub>O<sub>4</sub> magnetic core-shell nanocatalyst: Optimization, toxicity and degradation pathway studies. *Journal of Cleaner Production*, 192, 597–607. DOI 10.1016/j.jclepro.2018.04.274.
17. Tahir, M., Tahir, B., Zakaria, Z. Y., Muhammad, A. (2019). Enhanced photocatalytic carbon dioxide reforming of methane to fuels over nickel and montmorillonite supported TiO<sub>2</sub> nanocomposite under UV-light using monolith photoreactor. *Journal of Cleaner Production*, 213, 451–461. DOI 10.1016/j.jclepro.2018.12.169.
18. Wang, D., Liang, X., Li, D., Liang, H., Yu, H. (2018). Study on mechanics-based cracking resistance of semiflexible pavement materials. *Advances in Materials Science and Engineering*, 2018(11), 1–10. DOI 10.1155/2018/8252347.
19. Wang, K., Wu, P., He, J., Liu, C., Jiang, W. (2020). Evaluation of the engineering applications of superhydrophobic metal surfaces achieved by a spraying-adhering process using different combinations of hydrophobic particles and adhesives. *Industrial and Engineering Chemistry Research*, 59(42), 18873–18886. DOI 10.1021/acs.iecr.0c03546.
20. Morseletto, P. (2019). Confronting the nitrogen challenge: Options for governance and target setting. *Global Environmental*, 54, 40–49. DOI 10.1016/j.gloenvcha.2018.10.010.
21. Xie, R., Wei, D., Han, F., Lu, Y., Fang, J. et al. (2019). The effect of traffic density on smog pollution: Evidence from Chinese cities. *Technological Forecasting and Social Change*, 144, 421–427. DOI 10.1016/j.techfore.2018.04.023.
22. Li, Q., Jia, R., Shao, J., He, Y. (2019). Photocatalytic degradation of amoxicillin via TiO<sub>2</sub> nanoparticle coupling with a novel submerged porous ceramic membrane reactor. *Journal of Cleaner Production*, 209, 775–761. DOI 10.1016/j.jclepro.2018.10.183.
23. Hadnadjev-Kostic, M., Vulic, T., Marinkovic-Neducin, R., Loncarevic, D., Dostanic, J. et al. (2017). Photo-induced properties of photocatalysts: A study on the modified structural, optical and textural properties of TiO<sub>2</sub>-ZnAl layered double hydroxide-based materials. *Journal of Cleaner Production*, 164, 1–18. DOI 10.1016/j.jclepro.2017.06.091.

24. Fan, W., Chan, K., Zhang, C., Zhang, K., Ning, Z. et al. (2018). Solar photocatalytic asphalt for removal of vehicular NO<sub>x</sub>: A feasibility study. *Applied Energy*, 225, 535–541. DOI 10.1016/j.apenergy.2018.04.134.
25. Dou, Y., Jin, M., Zhou, G., Shui, L. (2015). Breath figure method for construction of honeycomb films. *Membranes*, 5(3), 399–424. DOI 10.3390/membranes5030399.
26. Gao, Z., Yang, H., Mao, J., Wu, J. (2019). Construction of  $\alpha$ -Fe<sub>2</sub>O<sub>3</sub> and Fe/Co-N<sub>4</sub> structures with faceted TiO<sub>2</sub> nanocrystals for highly efficient degradation of sulfathiazole in water. *Journal of Cleaner Production*, 220, 668–676. DOI 10.1016/j.jclepro.2019.02.168.
27. Guo, M., Li, J., Poon, C. S. (2019). Improved photocatalytic nitrogen oxides removal using recycled glass-nano-TiO<sub>2</sub> composites with NaOH pre-treatment. *Journal of Cleaner Production*, 209, 1095–1104. DOI 10.1016/j.jclepro.2018.10.303.
28. Leng, Z., Yu, H., Gao, Z. (2018). Study on air-purifying performance of asphalt mixture specimens coated with titanium dioxide using different methods. *International Journal of Pavement Engineering*, 11, 867–874. DOI 10.1016/j.ijprt.2018.08.003.
29. Luna, M., Gatica, J. M., Vidal, H., Mosquera, M. J. (2020). Use of Au/N-TiO<sub>2</sub>/SiO<sub>2</sub> photocatalysts in building materials with NO depolluting activity. *Journal of Cleaner Production*, 243, 118633. DOI 10.1016/j.jclepro.2019.118633.
30. Li, Q., Liu, Q., Peng, B., Chai, L., Liu, H. (2016). Self-cleaning performance of TiO<sub>2</sub>-coating cement materials prepared based on solidification/stabilization of electrolytic manganese residue. *Construction and Building Materials*, 106, 236–242. DOI 10.1016/j.conbuildmat.2015.12.088.
31. Nath, R. K., Zain, M. F. M., Jamil, M. (2016). An environment-friendly solution for indoor air purification by using renewable photocatalysts in concrete: A review. *Renewable & Sustainable Energy Reviews*, 62, 1184–1194. DOI 10.1016/j.rser.2016.05.018.
32. Yang, G., Su, J., Guo, Y., Xu, H., Ke, Q. (2017). Fabrication of TiO<sub>2</sub>/PI composite nanofibrous membrane with enhanced photocatalytic activity and mechanical property via simultaneous electrospinning. *Journal of Materials Science*, 52(9), 5404–5416. DOI 10.1007/s10853-017-0785-3.
33. Kim, Y. K., Hong, S. J., Kim, H. B., Lee, S. (2018). Evaluation of in-situ NO<sub>x</sub> removal efficiency of photocatalytic concrete in expressways. *KSCE Journal of Civil Engineering*, 22(7), 2274–2280. DOI 10.1007/s12205-017-0028-9.
34. Segundo, I. R., Dias, E. A. L., Fernandes, F., Freitas, E. F., Costa, M. F. M. et al. (2018). Photocatalytic asphalt pavement: The physicochemical and rheological impact of TiO<sub>2</sub> nano/microparticles and ZnO microparticles onto the bitumen. *Road Materials and Pavement Design*, 20(6), 1452–1467. DOI 10.1080/14680629.2018.1453371.
35. Segundo, I. R., Ferreira, C., Freitas, E. F., Carneiro, J. A. O., Fernandes, F. et al. (2018). Assessment of photocatalytic, superhydrophobic and self-cleaning properties on hot mix asphalts coated with TiO<sub>2</sub> and/or ZnO aqueous solutions. *Construction and Building Materials*, 166, 500–509. DOI 10.1016/j.conbuildmat.2018.01.106.
36. Fatima, R., Afridi, M. N. A., Kumar, V., Lee, J., Ali, I. et al. (2019). Photocatalytic degradation performance of various types of modified TiO<sub>2</sub> against nitrophenols in aqueous systems. *Journal of Cleaner Production*, 231, 899–912. DOI 10.1016/j.jclepro.2019.05.292.
37. Lyu, B., Cheng, K., Gao, D., Ma, J., Zhang, H. et al. (2019). Enhanced hygienic property of solvent-free polyurethane film by hollow TiO<sub>2</sub> microspheres. *Journal of Cleaner Production*, 209, 608–616. DOI 10.1016/j.jclepro.2018.10.282.
38. Shoueir, K., Kandil, S., El-hosainy, H., El-hosainy, M. (2019). Tailoring the surface reactivity of plasmonic Au@TiO<sub>2</sub> photocatalyst bio-based chitosan fiber towards cleaner of harmful water pollutants under visible-light irradiation. *Journal of Cleaner Production*, 230, 383–393. DOI 10.1016/j.jclepro.2019.05.103.